https://doi.org/10.5194/acp-2022-488
Preprint. Discussion started: 18 July 2022

Atmospheric Chemistry and Physics Discussions

Total ozone trends at three northern high-latitude stations

Leonie Bernet[1], Tove Svendby[1], Georg Hansen[1], Yvan Orsolini[1,2], Arne Dahlback[3], Florence Goutail[4], Andrea Pazmiño[4], Boyan Petkov[5,6], and Arve Kylling[1]

[1]NILU - Norwegian Institute for Air Research, Kjeller, Norway
[2]NTNU, Trondheim, Norway
[3]Department of Physics, University of Oslo, Oslo, Norway
[4]LATMOS/IPSL/USVSQ-CNRS, Guyancourt, France
[5]University G. d'Annunzio, Chieti-Pescara, Italy
[6]National Research Council, Institute of Polar Sciences (CNR-ISP), Bologna, Italy

Correspondence: Leonie Bernet (lber@nilu.no)

Abstract. After the decrease of ozone-depleting substances (ODSs) as a consequence of the Montreal Protocol, it is still challenging to detect a recovery in the total column amount of ozone (total ozone) at northern high-latitudes. To assess regional total ozone changes in the "ozone-recovery"-period (2000-2020) at northern high-latitudes, this study investigates trends from ground-based total ozone measurements at three stations in Norway (Oslo, Andøya, and Ny-Ålesund). For this purpose, we combine measurements from Brewer spectrophotometers, ground-based UV filter radiometers (GUVs), and a SAOZ instrument. The Brewer measurements have been extended to work under cloudy conditions using the global irradiance (GI) technique, which is also presented in this study. We derive trends from the combined ground-based time series with the multiple linear regression model from the Long-term Ozone Trends and Uncertainties in the Stratosphere (LOTUS) project. We evaluate various predictors in the regression model and found that tropopause pressure and lower-stratospheric temperature contribute most to ozone variability at the three stations. We report significant positive trends at Andøya (0.9% per decade) and Ny-Ålesund (1.5% per decade) and no annual trends at Oslo, but significant positive trends in autumn at all stations. Finally we found positive but insignificant trends of around 3% per decade in March at all three stations, which may be an indication for Arctic spring-time ozone recovery. Our results contribute to a better understanding of regional total ozone trends at northern high-latitudes, which is essential to assess how Arctic ozone responds to changes in ODSs and to climate change.

1 Introduction

As a consequence of the Montreal Protocol's success in reducing ozone-depleting substances (ODSs) in the stratosphere, the total column amount of ozone (total ozone) is expected to recover globally. A special focus lies on high latitudes, because they experienced the strongest stratospheric ozone depletion. Various studies showed that total ozone has started to recover in recent years in Antarctic spring (Solomon et al., 2016; Kuttippurath and Nair, 2017; Pazmiño et al., 2018; Weber et al., 2022). In the Arctic however, a recovery is more difficult to detect. Arctic recovery may be counteracted by climate change,

https://doi.org/10.5194/acp-2022-488
Preprint. Discussion started: 18 July 2022


Atmospheric Chemistry and Physics Discussions

because cooling and moistening of the stratosphere favours the formation of polar stratospheric clouds (PSCs) which may increase seasonal ozone depletion (von der Gathen et al., 2021). Furthermore, the strong interannual and dynamical variability at northern high-latitudes makes the trend detection challenging (e.g. Langematz et al., 2018). Given these challenges, several studies investigated Arctic spring total ozone and found no significant trends (Knibbe et al., 2014; Solomon et al., 2016; Weber et al., 2018, 2022).

Most of these trend studies concentrate on the whole Arctic area and do not account for regional variability. However, Coldewey-Egbers et al. (2022) recently reported distinct regional patterns in total ozone trends based on merged satellite data, especially at northern mid- to high-latitudes (40° N to 70° N). It is therefore crucial not only to investigate trends of zonal means, but to analyse regional trends at northern high-latitudes. Whereas satellites give a global picture of ozone trends, they have the disadvantage of drifts and limited lifetimes. Ground-based instruments on the other hand provide long-term and continuous measurements and are thus ideal to investigate regional ozone trends. Only few studies have investigated regional total ozone recovery at northern high-latitudes from ground-based measurements. Global total ozone trends from ground-based and satellite data including polar regions have been extensively investigated by Weber et al. (2018, 2022), but regional trend differences were not addressed. Trends at four Arctic stations derived from ozonesonde measurements were presented by Bahramvash Shams et al. (2019), but the analysis period was short (2005 to 2017) and ozonesonde launches are generally sparse. Svendby et al. (2021) presented ground-based trends at three Norwegian stations derived with a simple linear regression, but more advanced trend analyses for Norwegian stations have only been performed for the "ozone-depletion-period" (Svendby and Dahlback, 2004; Hansen and Svenøe, 2005).

The aim of our study is to investigate regional total ozone trends from ground-based measurements at three northern high-latitude stations in Norway (Oslo, Andøya and Ny-Ålesund). For this purpose, we combine measurements from Brewer spectrophotometers, ground-based UV filter radiometers (GUVs) and a SAOZ instrument (Sect. 2). In cloudy conditions or for low solar zenith angles (SZAs), we use Brewer measurements with the Global Irradiance (GI) method (Sect. 2.1.2), which is described in detail in Appendix A. Next, we compare our combined data with satellite overpasses and ERA5 reanalyses (Sect. 3). We then derive total ozone trends by using the multiple linear regression model provided by the Long-term Ozone Trends and Uncertainties in the Stratosphere (LOTUS) project (Sect. 4). The LOTUS regression was initially developed for global ozone profile trends at low- and mid-latitudes (SPARC/IO3C/GAW, 2019). We apply it for the first time on ground-based total ozone data at high latitudes. We therefore investigate the use of various regression predictors in the LOTUS model and define a set of predictors that explains the natural ozone variability at the three stations in the best possible way. Finally, the remaining and unexplained ozone changes are investigated and we present annual and monthly total ozone trends for the three stations (Sect. 5).

2 Total ozone data

In the present study we use total ozone data from three Brewer spectrophotometers, a SAOZ (Système d'Analyse par Observation Zénithale) instrument, and three Ground-based Ultraviolet radiometers (GUVs). Measurements are performed at

https://doi.org/10.5194/acp-2022-488
Preprint. Discussion started: 18 July 2022

Atmospheric Chemistry and Physics Discussions

Figure 1. Map of Europe showing the three measurement stations used in this study.

the Sverdrup station at Ny-Ålesund, Svalbard (78.92° N, 11.88° E, 15 m a.s.l.), at the Arctic Lidar Observatory for Middle Atmosphere Research (ALOMAR) on Andøya (69.28° N, 16.01° E, 360 m a.s.l.), and at Oslo (Blindern and Kjeller) (Fig. 1). Measurements at Oslo have been performed in Blindern (59.95° N, 10.72° E, 96 m a.s.l.) at the University of Oslo until July 2019, afterwards the instruments were moved to the Norwegian Institute for Air Research (NILU) in Kjeller (59.98° N, 11.05° E, 139 m a.s.l.), which is located around 18 km east of Blindern. We have co-located Brewer and GUV measurements at all stations, and additional SAOZ measurements at Ny-Ålesund. All instruments provide data in the full study period (2000 to 2020), except the Brewer at Ny-Ålesund that has been operating since 2013. Measurement availability depends on season and technique as described below.

2.1 Brewer spectrophotometers

We use ozone data from three Brewer spectrophotometers that measure UV radiation between 305 and 320 nm. The Brewer located at Oslo is a single-monochromator Brewer MKV (serial number B42), whereas a double-monochromator Brewer MKIII (B104) is located at Andøya. Both instruments are operated by NILU and have been calibrated every summer by the International Ozone Service (IOS, Canada). No calibrations were performed in 2020 and 2021 due to travel restrictions related to the COVID-19 pandemic. The Brewer at Ny-Ålesund is operated by the National Research Council, Institute of Polar Sciences (CNR-ISP), Italy. It has been calibrated by IOS in 2015 and 2018. The Brewer calibration dates are given at

https://doi.org/10.5194/acp-2022-488
Preprint. Discussion started: 18 July 2022

Atmospheric Chemistry and Physics Discussions

https://www.io3.ca/Calibrations. We investigated all calibration reports and performed some changes in the calibration files. The updates were small (mainly small calibration date corrections) and affected only a few single days. Measurements during the whole calibration period were excluded.

2.1.1 Direct sun method

For the default direct sun (DS) measurements, the Brewer instrument measures direct sunlight in the UV, as described for example in Savastiouk and McElroy (2005). Total ozone is then derived from the intensities by considering ozone absorption coefficients and Rayleigh scattering coefficients (e.g. Fioletov et al., 2011), using the O3Brewer-software (version 6.6 available at http://www.o3soft.eu/o3brewer.html). All DS measurements are regularly calibrated with standard lamp (SL) measurements. For the SL-correction, the intensities of an internal halogen lamp are measured at the same five wavelengths as for the ozone measurements. The SL produces a stable and continuous light spectrum. Any variations visible in the SL-measurements would also affect the ozone measurements and are therefore corrected therein.

2.1.2 Global irradiance method

The DS method is limited to clear-sky conditions and solar zenith angles (SZA) below 72°. Therefore, we use the global irradiance (GI) method to retrieve ozone in cloudy conditions and/or for larger SZA at Oslo and Andøya. In contrast to the DS method, the GI method relies on measurements of diffuse and direct irradiance, including multiple scattering due to clouds and surface reflection. A detailed description of the method is given in Appendix A. The same method has recently been used to derive total ozone from Ground-based UV radiometers by Svendby et al. (2021).

To validate the GI measurements, we compared GI daily means with coincident reanalysis data (ERA5, see Sect. 2.6) at Andøya (Fig. 2). In addition, we show data from the Zenith Sky (ZS) method that is commonly used to retrieve ozone in cloudy conditions (e.g. Fioletov et al., 2011). We observe a good agreement with ERA5 data, with an average absolute difference between ERA5 and GI of 2.3±2.5% at Andøya (Fig. 2) and 2.2±2.1% at Oslo (not shown). We further observe that GI measurements agree slightly better with ERA5 than ZS measurements, especially at Andøya.

Fig. 2 also shows the SL measurements at Andøya for the two SL ratios R5 and R6 and shows large changes in the standard lamp in Andøya between 2015 and 2018. The good agreement with ERA5 data also in these years illustrates that such irregularities can be handled thanks to the regular calibrations and the SL correction in the GI retrieval (see Appendix A2).

Our results show that the GI method can provide ozone data of higher quality than the commonly used ZS method. The advantage of GI is that it can also be used at high SZA, and the measurement season at high latitudes can therefore be extended in winter months when the sun is low. Furthermore, the GI method is based on physical measurements, whereas the ZS method is normally based on purely statistically derived relationships.

https://doi.org/10.5194/acp-2022-488
Preprint. Discussion started: 18 July 2022

Atmospheric Chemistry and Physics Discussions

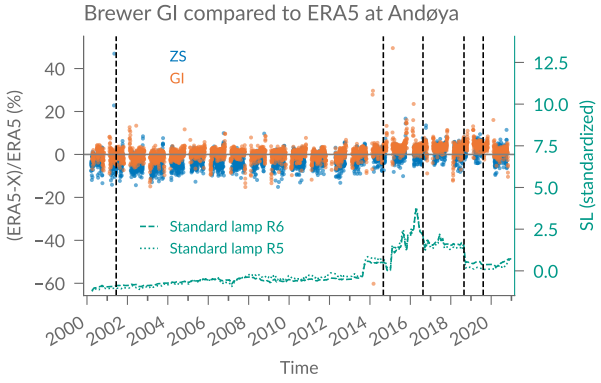

Figure 2. Brewer Global Irradiance (GI) data compared to ERA5 data at Andøya. Brewer Zenith sky (ZS) data are shown in addition. The right axis shows standard lamp (SL) ratios R5 and R6, standardized to zero mean and standard deviation of one. Vertical dashed lines show dates that were used for GI calibration at Andøya.

2.2 GUV

The ground-based UV (GUV) filter radiometers in Oslo (type GUV-511), Andøya, and Ny-Ålesund (both type GUV-541) measure direct and diffuse solar irradiance at five channels in the UV range from 305 to 380 nm. The measurements are used to derive the UV index, total ozone, biological doses, and cloud transmittance (Svendby et al., 2021). Detailed information about the GUV instruments and the measurement technique can be found in Bernhard (2005) and Svendby et al. (2021). Our GUV data corrections for seasonality and clouds are performed as described by Svendby et al. (2021). In addition, we restrict the data from February to October in Andøya and from March to September in Ny-Ålesund, due to limited measurement days in the winter months caused by the low sun or polar night.

2.3 SAOZ

The Système d'Analyse par Observation Zénithale (SAOZ) instrument at Ny-Ålesund measures solar radiation in the UV-visible range of the solar spectrum (300–650 nm). Its measurement principle and basic instrument setup is described in Pommereau and Goutail (1988). Total ozone is retrieved from the measured slant columns at sunrise and sunset, when the SZA is between 86° and 91° (Goutail et al., 2005). In order to convert measured slant columns to vertical columns, ozone air mass factor (AMF) lookup tables are used, calculated using the TOMS V8 ozone profiles (Hendrick et al., 2011). SAOZ ozone measurements present a precision of 4.7% and an accuracy of 5.9%. No measurements are available in summer when the SZA is high, and we use SAOZ data only in spring (March and April) and autumn (August and September).

https://doi.org/10.5194/acp-2022-488
Preprint. Discussion started: 18 July 2022

Atmospheric Chemistry and Physics Discussions

Figure 3. Daily means of total ozone from four different measurement techniques: Brewer Direct Sun (DS), Brewer Global Irradiance (GI), ground-based UV (GUV), and SAOZ, measured at **(a)** Oslo, **(b)** Andøya, and **(c)** Ny-Ålesund. DS data are the main dataset in Oslo **(a)** and Andøya **(b)**, days without DS measurements are filled with GI data, remaining missing data are then filled with GUV measurements. In Ny-Ålesund **(c)**, SAOZ is the main dataset, and DS and GUV are used to fill days with missing SAOZ data.

2.4 Combined ground-based total ozone data

To obtain ground-based total ozone time series with as few missing measurement days as possible, we combine total ozone measurements from the four different measurement techniques to a combined time series (GBcomb). The Brewer DS measurements build the baseline in Oslo (53% of the measurement days) and Andøya (44%). Missing measurement days are first filled with GI data (around 40% at both stations), then with GUV (5% in Oslo and 15% in Andøya) (Fig. 3a,b). In Ny-Ålesund (Fig. 3c), we use SAOZ data as the baseline (around 35% of the measurements), and days without SAOZ measurements (mainly during summer) are filled with Brewer data (20% starting in July 2013), and with GUV data (45% after 2013). In Oslo we have data throughout the year, whereas we have measurements from February or March to October in Andøya. The combined time series at Ny-Ålesund is available from February or March to September or October, depending on the year. For each instrument, we compute daily means of total ozone measurements by considering measurements $\pm$2h around local noon. Only for SAOZ, daily means of sunset and sunrise measurements are used. Local noon is approximated by the longitude of the station, and is 11:15 UTC at Kjeller, 10:55 UTC at Andøya and 11:12 UTC at Ny-Ålesund. Outliers are excluded when the daily standard deviation exceeds ten times the mean standard deviation or if the daily mean exceeds four times the score z, where $z = (O_3 - \overline{O}_3)SD^{-1}$, with the overall mean ozone $\overline{O}_3$ and the overall standard deviation SD.

https://doi.org/10.5194/acp-2022-488
Preprint. Discussion started: 18 July 2022


Atmospheric Chemistry and Physics Discussions

2.5 Satellites

We use daily means of satellite overpass data from the Ozone Monitoring Instrument (OMI) on the Aura satellite (OMDOAO3 product) launched in 2004 and from two Global Ozone Monitoring Experiment-2 (GOME-2) instruments on the satellites Metop-A (GOME-2A, launched in 2006) and Metop-B (GOME-2B, launched in 2012). In addition we use daily overpass data from the Solar Backscatter ultraviolet (SBUV) Merged Ozone Dataset (MOD) (SBUV MOD version 2 release 1), which combines total ozone measurements from several SBUV instruments (Frith et al., 2014) processed with a single retrieval algorithm (version 8.7).

2.6 ERA5

We use 2-hourly data on single levels of ERA5, the atmospheric reanalysis from the European Centre for Medium Range Weather Forecasts (ECMWF) (Hersbach et al., 2018, accessed on 2021-03-24). Various total ozone satellite products are assimilated in ERA5, as described by Hersbach et al. (2020). We use ERA5 data at 10:00 and 12:00 UTC for the grid point closest to each station.

3 Time series comparison

The comparison between the combined ground-based time series (GBcomb), ERA5 reanalysis data and satellite overpasses is shown in Fig. 4. The GBcomb monthly means are shown in the first row of Fig. 4, complemented by ERA5 data to fill the seasonal measurement gaps (Fig. 4a-c). The strong seasonal cycle and the interannual variability is clearly visible at all stations. We can also see the measurement season of our ground-based data, with missing GBcomb data in winter months at Andøya and Ny-Ålesund. The second row in Fig. 4(d-f) shows the deviation from the climatology (2000-2020), the so-called anomalies. These deseasonalized monthly means show that total ozone varies naturally within around 10% at Oslo (Fig. 4d) and 20% at Andøya (Fig. 4e) and Ny-Ålesund (4f). The datasets generally agree on the natural variability and the anomalies, with larger anomalies in some years. For example, the ozone-poor year 2020 in the Arctic is clearly visible at Ny-Ålesund (Fig. 4f). Also, the strong negative anomaly in 2011 can be seen in all datasets at all stations. However, we observe that ERA5 reports more total ozone than the other datasets at all stations starting in 2014.

Finally, we compare differences between GBcomb, satellites and ERA5. For this, we compare daily ground-based measurements with coincident satellite overpasses and ERA5 data and show the monthly means of these differences for each station (Fig. 4g-i). On average, we observe absolute differences of 1 to 3% at all stations. This agrees with satellite uncertainties of around 2% as reported by Bodeker and Kremser (2021). We observe larger deviations for single months, but differences are never larger than 9%. In Andøya we observe a drift compared to some satellites from 2014 to 2016, and we observe a drift in opposite direction in Ny-Ålesund starting in 2016. The drifts occur mainly compared to GOME2 and ERA5 and are less visible compared to OMI and SBUV. Further analyses would be required to investigate these differences. Interestingly, all satellites underestimate ozone at Ny-Ålesund in the extreme spring 2020 compared to the ground-based data.

https://doi.org/10.5194/acp-2022-488
Preprint. Discussion started: 18 July 2022

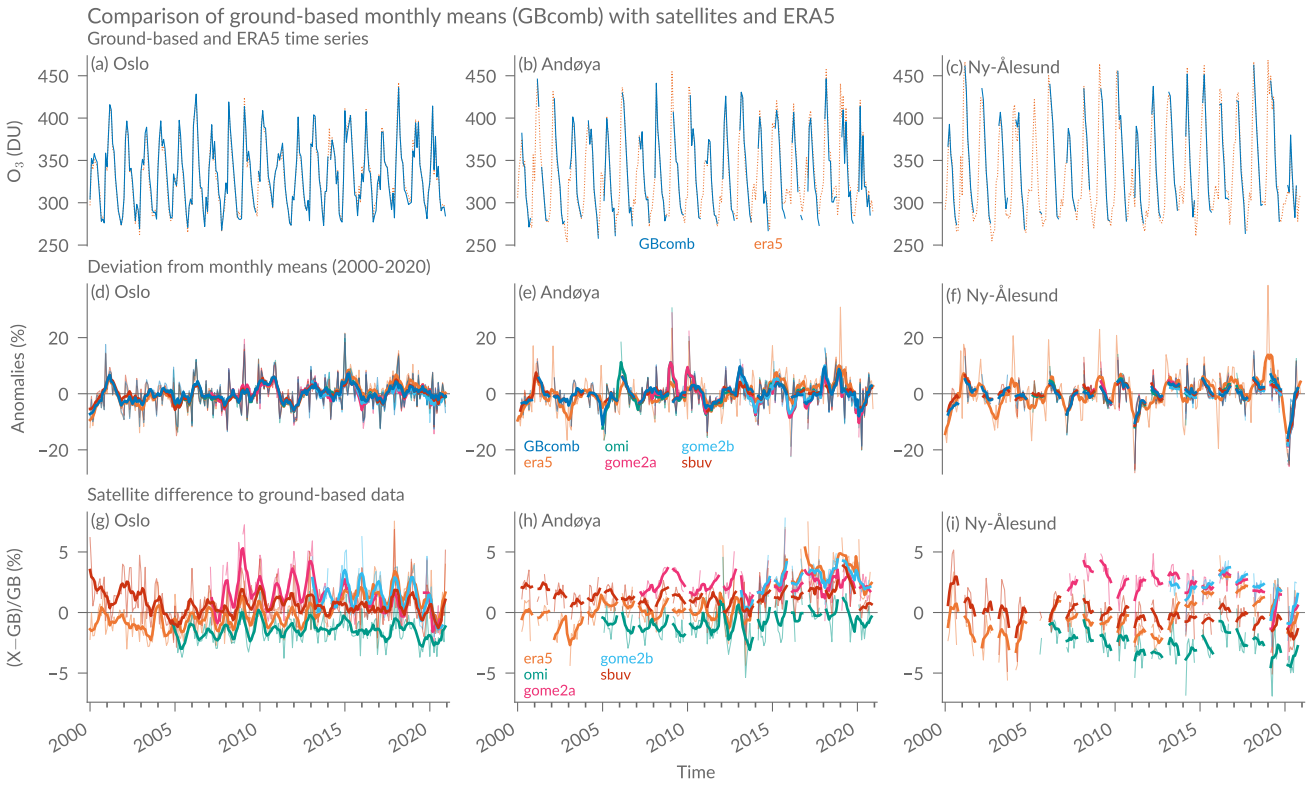

Figure 4. Comparison of the combined ground-based data (GBcomb) with satellite overpasses and ERA5 data at the three stations Oslo, Andøya and Ny-Ålesund. The first row (**(a)–(c)**) shows monthly means of the ground-based data together with ERA5 monthly means. The second row (**(d)–(f)**) shows relative anomalies for each dataset, which are defined as the deviation of each month from the monthly mean climatology (2000–2020) of the respective dataset. The third row (**(g)–(i)**) shows monthly differences between GBcomb and coincident daily means of the other datasets. The thick lines in **(d)–(i)** show data smoothed with a moving window of 6 months (with a minimum window size of 3 months).

4 Multiple linear regression

We use a multiple linear regression model that was developed within the activity Long-term Ozone Trends and Uncertainties in the Stratosphere (LOTUS). The so-called LOTUS regression has been tested with several ozone datasets and is described in detail in SPARC/IO3C/GAW (2019). We use the model version 0.8.0 (USask ARG and LOTUS Group, 2017) and extended it by adding additional predictors (see Sect. 4.1). The following regression function is used:

$$\hat{y}(t) = a + b \cdot t + \sum_{n=1}^{4} \left(c_n \cdot \sin\left(\frac{2\pi}{l_n} \cdot t\right) + d_n \cdot \cos\left(\frac{2\pi}{l_n} \cdot t\right) \right) + \sum_{n=1}^{m} (\beta_n X_n) \quad (1)$$

https://doi.org/10.5194/acp-2022-488
Preprint. Discussion started: 18 July 2022


Atmospheric Chemistry and Physics Discussions

with the estimated ozone time series $\hat{y}(t)$, the time vector of monthly means t, a constant intercept a and a linear term b. The seasonal cycle is considered by adding annual oscillations and some overtones (l_n = 12, 6, 4, and 3 months), with fitted coefficients c_n and d_n. In addition, we include m explanatory variables X_n and their fitted coefficients β_n to explain natural variability of ozone. At Ny-Ålesund, only two seasonal components are used (l_n = 12, 6 months) due to the incomplete seasonal cycle because of missing measurements in winter. The regression coefficients are determined by minimizing a cost function, whereas uncertainties of the time series are considered in a full error covariance matrix. The model is iteratively corrected for autocorrelation according to the method by Cochrane and Orcutt (1949) (Damadeo et al. (2014, Appendix B), SPARC/IO3C/GAW (2019)).

The regression is applied to monthly means from the combined daily ozone data (GBcomb). We exclude months with less than 25 measurement days to avoid values that are not representative for the whole month. This implies that at Andøya monthly means are excluded for February in several years and from November to January in all years, and at Ny-Ålesund from October to February. Monthly ozone uncertainties are considered in the error covariance matrix, using the standard error SE of each monthly mean ($SE = \sigma_m \, n^{-\frac{1}{2}}$, with σ_m the standard deviation of the daily measurements for a particular month and n the number of measurement days for that month). We start our trend analyses in the year 2000, when a general turnaround in ODSs is assumed in polar regions (SPARC/IO3C/GAW, 2019; Weber et al., 2018; Newman et al., 2007; WMO, 2018).

4.1 Regression predictors

The aim of the regression is to assign as much ozone variability as possible to known natural variability by including various predictors. By including the predictors in the regression without detrending them, any trend that is due to long-term changes in one of the predictors is removed from the ozone time series. The remaining, unexplained trend is then assumed to be due to changes in ODSs. The LOTUS regression was initially designed to derive stratospheric trend profiles for a broad set of global satellite data (SPARC/IO3C/GAW, 2019). Predictors were selected to obtain a regression that performs best in this setting. The default predictors in the LOTUS regression are: the El Niño Southern Oscillation (ENSO) (e.g. Oman et al., 2013), the Quasi-Biennial Oscillation (QBO) (e.g. Baldwin et al., 2001), solar flux at 10.7cm wavelength (e.g. Lee, 2003), and aerosol optical depth (AOD, e.g. Solomon et al. (1998)). However, additional predictors may be required when using the regression for local stations, as suggested by Van Malderen et al. (2021) and SPARC/IO3C/GAW (2019). A few recent studies used the LOTUS regression to derive local trend profiles at specific stations (Godin-Beekmann et al., 2022; Bernet et al., 2021; Van Malderen et al., 2021), but they did not investigate the use of additional local predictors. Furthermore, all studies using the LOTUS regression concentrate on latitudes between 60° S and 60° N and on stratospheric ozone profiles. For total ozone trends at higher latitudes, as investigated in our study, other dynamical and chemical predictors can influence ozone variability. A detailed overview about potential predictors that influence total ozone is given for example by Mäder et al. (2007). Various studies investigated how such predictors can be used in multiple linear regressions to derive trends at high latitudes (e.g. Knibbe et al., 2014; Kuttippurath et al., 2015; De Laat et al., 2015; Weber et al., 2022; Pazmiño et al., 2018). We investigate the use of the most relevant predictors in addition to the LOTUS default predictors. For some of them we use local data at the specific stations, and those with a strong seasonal cycle are deseasonalized, as indicated in Table 1.

https://doi.org/10.5194/acp-2022-488
Preprint. Discussion started: 18 July 2022

Atmospheric Chemistry and Physics Discussions

Table 1. Predictors investigated for use in the multiple linear regression. Predictors that have been used in the final regression are marked in bold.

Predictor	Full predictor name	Data and Source
ENSO	El Niño Southern Oscillation	Multivariate ENSO index (version 2) derived from five surface variables. https://www.esrl.noaa.gov/psd/enso/mei/data/meiv2.data
QBO(a-d)	Quasi-Biennial oscillation	Four principal components of equatorial wind at 7 pressure levels (70, 50, 40, 30, 20, 15, 10 hPa). https://www.geo.fu-berlin.de/met/ag/strat/produkte/qbo/qbo.dat
Solar	Solar flux	Adjusted solar index at 10.7 cm from OMNI. https://omniweb.gsfc.nasa.gov/form/dx1.html
AOD	Aerosol optical depth	Aerosol Extinction coefficients at 525nm from GloSSAC/NASA. Use constant after 12-2018 (last measured value). https://asdc.larc.nasa.gov/project/GloSSAC/GloSSAC_2.0
AO	Arctic oscillation	Monthly mean index from NOAA. http://www.cpc.ncep.noaa.gov/products/precip/CWlink/daily_ao_index/monthly.ao.index.b50.current.ascii
NAO	North Atlantic oscillation	Monthly mean index from NOAA. http://www.cpc.ncep.noaa.gov/products/precip/CWlink/pna/norm.nao.monthly.b5001.current.ascii
EHF	Mean Eddy heat flux	Heat flux at 100hPa from MERRA2 reanalysis, averaged over 45° N to 75° N, cumulative mean from September to April, deseasonalized. https://acd-ext.gsfc.nasa.gov/Data_services/met/ann_data.html
T50*	Stratospheric temperature	Deseasonalized temperature at 50hPa from ERA5 reanalysis at each station. Hersbach et al. (2019, accessed on 2021-09-03)
TropP*	Tropopause pressure	Deseasonalized data from NCEP reanalysis (Kalnay et al., 1996) at each station. ftp://ftp.cdc.noaa.gov/Datasets/ncep.reanalysis.derived/tropopause/pres.tropp.mon.mean.nc
TropT*	Tropopause temperature	Deseasonalized data from NCEP reanalysis (Kalnay et al., 1996) at each station. ftp://ftp.cdc.noaa.gov/Datasets/ncep.reanalysis.derived/tropopause/air.tropp.mon.mean.nc
VPSC	Volume of polar stratospheric clouds	Deseasonalized Polar stratospheric Cloud (PSC) NAT (nitric acid trihydrate) volume derived from MERRA2. https://ozonewatch.gsfc.nasa.gov/meteorology/temp_2020_MERRA2_NH.html

* Local station-specific data were used for those predictors.

For total ozone, tropopause properties are especially important, as the position of the tropopause has a strong influence on the column amount of ozone (e.g. Wohltmann et al., 2005; Varotsos et al., 2004). An increase in tropospheric height has been recently reported (Thompson et al., 2021; Meng et al., 2021), which may influence ozone trends and should thus be considered in the regression. We therefore investigate the use of station-specific tropopause pressure (TropP) and tropopause temperature (TropT) as predictors. Further, chemical ozone destruction at high latitudes is strongly linked to stratospheric temperature and the occurrence of polar stratospheric clouds (PSCs). We thus inspect the use of a stratospheric temperature predictor at 50hPa (T50) and an estimator of the PSC volume (VPSC). We also examine the use of some northern teleconnection patterns, namely the Arctic oscillation (AO) and the North Atlantic oscillation (NAO). Such dynamical patterns can have an important effect on total ozone (e.g. Orsolini and Doblas-Reyes, 2003; Appenzeller et al., 2000; Brönnimann et al., 2000). The Brewer-Dobson

https://doi.org/10.5194/acp-2022-488
Preprint. Discussion started: 18 July 2022


Atmospheric Chemistry and Physics Discussions

circulation (BDC) plays an important role in explaining natural ozone variability, especially at high latitudes (e.g. Plumb, 2002). Its strength can be characterized by the upward propagation of planetary waves, represented by the meridional eddy heat flux (EHF) (e.g. Gabriel and Schmitz, 2003). We therefore include the mean EHF at 100hPa pressure level averaged over 45° N to 75° N as a measure of the strength of the BDC. The BDC transports ozone-rich air from the tropics towards the winter pole, and the EHF is strongest in winter. However, the transport-related variability affects not only ozone in winter and spring, but can influence the amount of ozone until the following autumn (Fioletov and Shepherd, 2003). We therefore compute a cumulative mean from September to April, as suggested by Weber et al. (2018). Starting in September, each monthly EHF value is computed by averaging from September until the current month. The cumulated cold season mean (September to April) is then also used in the warm season, from May to August.

Finally, we made some adjustments to the default use of QBO terms in the LOTUS regression. The QBO predictor is based on equatorial wind measurements at 7 pressure levels. These equatorial oscillations affect ozone beyond the tropics up to polar regions (Wang et al., 2022). However, amplitude, phase and frequency of the QBO signal may change at higher latitudes (Damadeo et al., 2014). The phase- and amplitude changes can be considered by using principal components of the 7 pressure levels rather than using the direct QBO time series (Damadeo et al., 2014; SPARC/IO3C/GAW, 2019). We use the four leading principal components (QBOa-d) as suggested by Damadeo et al. (2014). Only two components were used in the LOTUS regression so far, but Anstey et al. (2021) showed that additional components are necessary to capture the recent QBO disruption in northern-hemisphere winter 2019/2020. Furthermore, we added two seasonal components to the QBO predictors. This is important, because a seasonal dependence of QBO is observed at higher latitudes (Tung and Yang, 1994; Damadeo et al., 2014), which is generally not captured by regression models (Ball et al., 2019). Also, Godin-Beekmann et al. (2022) showed that the regression fit improves when seasonal components of predictors are included in the LOTUS regression.

4.2 Final choice of predictors

A multiple linear regression is based on the assumption that the predictors are independent. For our final selection of predictors, we therefore investigate the predictors' correlations. The Pearson correlation coefficient r for all the predictors that we investigated at Oslo are shown in Fig. 5. The significance of each coefficient has been tested with a p-value of 0.05, using a multiple test to reduce the possibility that a correlation is significant by chance (adjusted p-value). Some predictors can immediately be excluded because of their high correlation to another predictor. For example, tropopause pressure (TropP) and tropopause temperature (TropT) should not be used both because they are significantly correlated ($r = 0.91$). We decide to use TropP and not TropT, because the tropopause altitude has a large influence on total ozone (e.g. Steinbrecht et al., 1998; Varotsos et al., 2004). Furthermore, the circulation patterns NAO and AO are significantly correlated (r =0.62) and should not be used both in the regression. TropP and T50 are also significantly correlated ($r = 0.51$), but their simultaneous use is further discussed below. Finally, there is a significant correlation between AOD and the solar flux ($r = -0.51$). This might be a spurious correlation in the selected time period, where AOD was generally low because no major volcanic eruption occurred. Indeed, no correlation between solar flux and AOD is observed for a longer time period from 1979 to 2020 (not shown). The ozone effect from AOD

https://doi.org/10.5194/acp-2022-488
Preprint. Discussion started: 18 July 2022

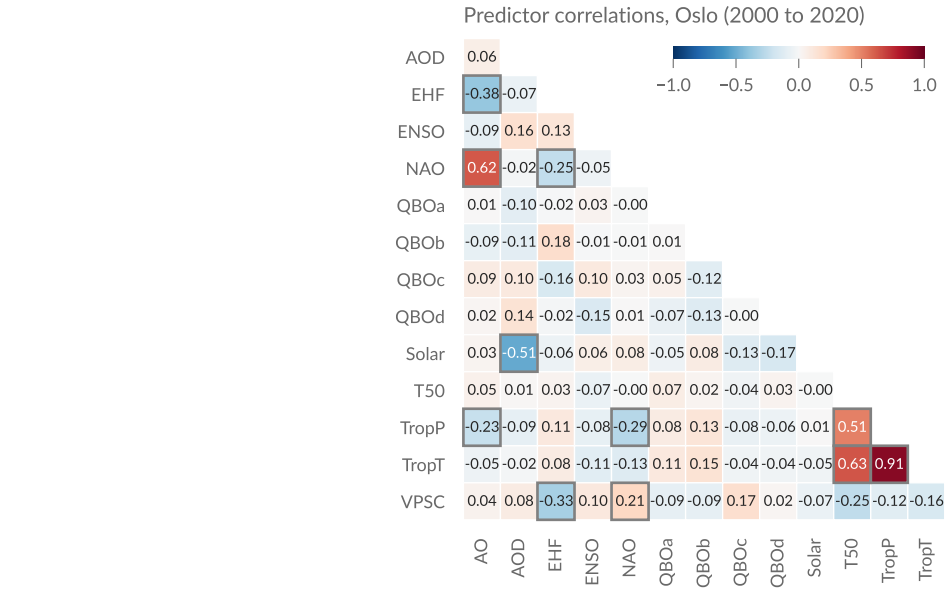

Figure 5. Pearson correlation coefficients of various predictors that are commonly used to account for natural ozone variability. The predictors that are location-specific are shown for Oslo (TropP, TropT and T50), the other predictors are station-independent. Significant correlations are marked with a grey border. The significance has been tested with a p-value of 0.05 using a multiple test to reduce the possibility that a correlation is significant by chance (adjusted p-value).

is mainly relevant for important volcanic eruptions (e.g. Solomon et al., 1998) and we therefore decide not to use AOD in our regression.

Besides the independence and the physical meaningfulness of the predictors, it is important to study the improvement of the regression fit when a specific predictor is included. Based on these aspects, we decided on a final set of predictors used in the regression fit. First, we decided to use T50, even though it is correlated to TropP, because including T50 substantially improves the adjusted coefficient of determination (R^2_{adj}) of the model fit (e.g. from 0.91 to 0.96 at Oslo). To be sure that the correlation between both does not affect the interpretation of our results, we also inspected the fit for a possible multicollinearity by investigating the variance inflation factor (VIF). We used a VIF threshold of 5, which means that no collinearity problem is assumed when testing the regression with each predictor as dependent variable as long as VIF<5 (e.g. Schuenemeyer and Drew, 2010). We observed multicollinearity only for monthly trends at Oslo in March ($VIF_{TropP} = 5.2$) and September ($VIF_{T50} = 5.5$) and at Ny-Ålesund in September ($VIF_{TropP} = 5.0$), but not for full trends.

Second, we decided not to include the dynamical predictors NAO and AO, because they are weakly but significantly correlated with TropP and EHF (Fig. 5). These large-scale predictors should be well represented in the local predictors (TropP), as also suggested by Mäder et al. (2007). Also, there is no important improvement in the model performance when NAO and AO predictors are included. Finally, we do not include VPSC because of the weak but significant correlation to EHF (Fig. 3),

https://doi.org/10.5194/acp-2022-488
Preprint. Discussion started: 18 July 2022

Atmospheric Chemistry and Physics Discussions

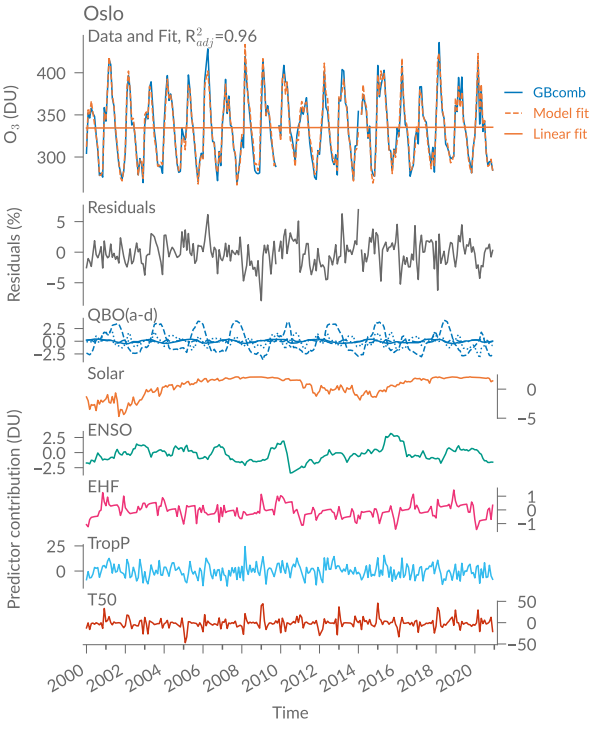

Figure 6. Regression fit, residuals and predictor contribution ($\beta_n \cdot X_n$, with coefficient β_n and predictor X_n) at Oslo.

even though we observe that the fit residuals are improved in some extreme years when VPSC is included at Ny-Ålesund (not shown). The chosen predictors that are finally used in the regression are marked in bold in Table 1.

Figure 6 shows the contribution of the selected predictors to the regression fit at Oslo using the full time series, further referred to as full trend fit. The model is well representing the data with a R^2_{adj} of 0.96, which indicates that the regression fit can explain 96% of the ozone variation at Oslo. The residuals generally lie within 5% and a spectral analysis of the residuals (not shown) suggests that the dominant patterns that influence ozone variation are captured by the regression. The lower panels in Fig. 6 show that most of the ozone variation can be explained by T50 and TropP (predictors with largest contribution), followed by two of the QBO-terms (QBOb and QBOc). The solar flux, ENSO and EHF have only small contributions to ozone variability at Oslo. However, all predictors have a significant contribution to the regression fit except the EHF and 3 of the QBO components (see full fit in Fig.7). At Andøya and Ny-Ålesund, the EHF contribution to the full fit is significant, but some of the default predictor coefficients (Solar, ENSO and QBO) become insignificant (see Figs. B1 and B2), which confirms results by Bahramvash Shams et al. (2019) based on ozonesonde measurements in the Arctic.

The predictor coefficients, their significance, and the model's performance for individual monthly fits at Oslo are shown in Fig.7. The coefficients have been standardized to make a direct comparison possible. The standardized coefficients β_{std}

https://doi.org/10.5194/acp-2022-488
Preprint. Discussion started: 18 July 2022

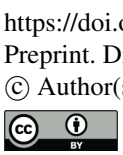

Atmospheric Chemistry and Physics Discussions

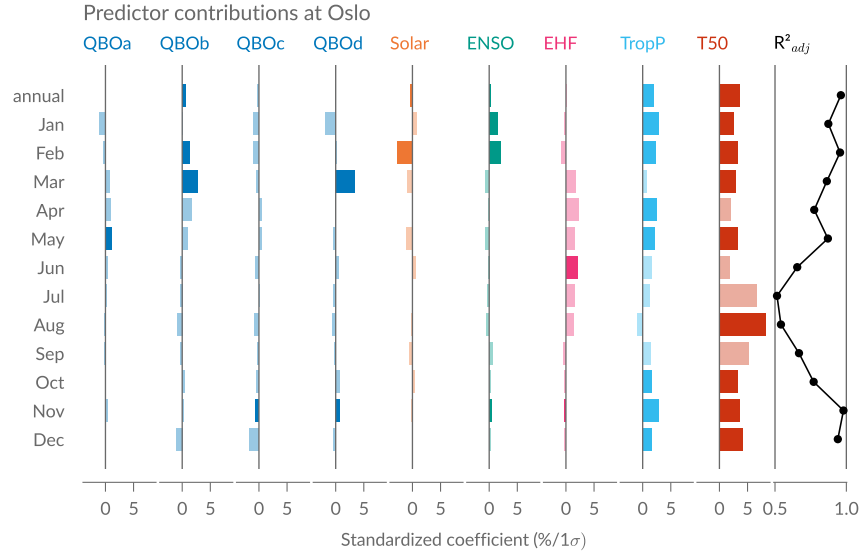

Figure 7. Predictor contribution to the regression fit at Oslo for the full annual regression fit and individual monthly fits. The standardized coefficients describe the percentage change in ozone for a 1-standard-deviation change in the predictor. Pale color bars indicate that the predictor's contribution to ozone is not significant (p-value of the coefficient <0.05). The last panel on the right shows the adjusted coefficient of determination (R^2_{adj}) for the annual and all monthly fits.

describe the percentage change in ozone for a 1-standard-deviation change in the predictor, according to Brunner et al. (2006):

$$\beta_{std} = \beta \frac{\sigma_X}{\bar{y}} \cdot 100 \tag{2}$$

with the predictor coefficient β, the standard deviation σ_X of predictor X and the mean ozone value $\bar{y}$. Generally, the largest contribution to total ozone is provided by the T50 predictor, followed by TropP (Fig. 7). Whereas most predictors contribute significantly to the full regression fit and to most monthly fits in winter, the regression coefficients are mostly insignificant in the summer months (pale shading in Fig. 7). This poor explanation of ozone variability in summer by the predictors is reflected in lower values of R^2_{adj} from June to September (R^2_{adj} between 0.5 and 0.7), with particular low values in July and August (0.51 and 0.54). In most other months, however, the ozone variation at Oslo is well captured by the model, with R^2_{adj} ranging from 0.77 (October) to 0.98 (November). Total ozone in summer is generally driven by photochemistry and less by the transport-related predictors, which may explain the poorer model performance in summer. Furthermore, the interannual variability is generally low in summer and may be dominated by noise, as suggested by Brunner et al. (2006).

In Ny-Ålesund and Andøya, we observe high R^2_{adj} in March and September and smaller values in the other months, especially in April (both stations) and May (only at Ny-Ålesund) (see Figs. B1 and B2). However, the R^2_{adj} at those stations is generally lower than in Oslo, especially at Ny-Ålesund. This can be explained by the high interannual variability at Andøya and Ny-Ålesund (compare Fig. 4e,f) that makes it more difficult to explain the ozone variability with the predictors used.

https://doi.org/10.5194/acp-2022-488
Preprint. Discussion started: 18 July 2022


Atmospheric Chemistry and Physics Discussions

5 Trend results

5.1 Full trends

Full trend fits (using the full time series) and their residuals for the three stations are shown in Fig. 8. At all stations, we observe that the model represents the data well, with R^2_{adj} values of 0.96 (Oslo and Andøya) and 0.97 (Ny-Ålesund). The residuals lie within 5%, with some outliers of up to 10% in Andøya and Ny-Ålesund, where the model captures less well the ozone variability (e.g. in 2008 or 2020). The standard errors of the residuals (SE_{res}) of 1.24 DU (Oslo) to 1.62 DU (Ny-Ålesund) also indicate a good model performance. We observe significant positive total ozone trends at Andøya and Ny-Ålesund of 0.9 and 1.5% per decade respectively, and a trend of almost zero (0.1% per decade) at Oslo (see Fig. 8). Trends are expressed as percentage of the mean ozone value at each station and a trend is declared to be significantly different from zero at a 95 % confidence interval as soon as its absolute value exceeds twice its uncertainty (e.g. Tiao et al., 1990).

Positive trends of similar magnitudes have also been found for Scandinavia or the North Atlantic in previous satellite-based studies. For example, Sofieva et al. (2021) found positive trends over Scandinavia at several altitudes based on merged satellite ozone profile data from 2003 to 2018 (their Fig. 10), and Coldewey-Egbers et al. (2022) reported significant positive total ozone trends in the North Atlantic sector based on merged total ozone data from 1997 to 2020 (their Fig. 3). Using ground-based GUV measurements at the same three stations as in our study, Svendby et al. (2021) analysed total ozone trends based with a simple linear regression from 1999 to 2019. They found similar positive trends, but slightly larger uncertainties. In contrast to our results at Andøya and Ny-Ålesund, their annual trends were not significant, which suggests that the use of multiple predictors in our study can successfully reduce trend uncertainties at the two northernmost stations.

5.2 Monthly trends

Monthly trends were computed for all stations by applying the regression to the time series of each month, usually including 21 data points for each month (2000 to 2020). We do not include February trends at Andøya because the time series is short (only 15 years) due to sparse February measurements in some years. The monthly regression analysis results in significant positive ozone trends in autumn at Oslo (October: 2.4±1.5% and November: 1.4±0.7% per decade) and in late summer/autumn at Andøya (August: 2.5±2.0%) and Ny-Ålesund (September: 3.5±2.8% per decade), as illustrated in Figure 9. Trends in other months are not significantly different from zero at 95% confidence interval, except a significant negative trend at Oslo in February (-4.3±2.2% per decade). From May to August, Oslo trends are almost zero and insignificant. The same is the case at Andøya from June to October, except in August for which we observe a significant positive trend.

In Winter (December to February), we only derive trends in Oslo due to the missing data (polar night) at the other stations. Winter Oslo trends are positive but insignificant in December and January, and significantly negative in February. The negative February trend in Oslo persists even if we exclude the extreme year 2020 from the regression. This negative trend may be specific for the selected time period: in the first five years (2000-2005) we have rather stable February monthly means, afterwards we observe more interannual variability and several years with specially low ozone, which results in a negative trend (not shown). Furthermore, we observe that the periods with less variable February values seem to coincide with the solar

https://doi.org/10.5194/acp-2022-488
Preprint. Discussion started: 18 July 2022

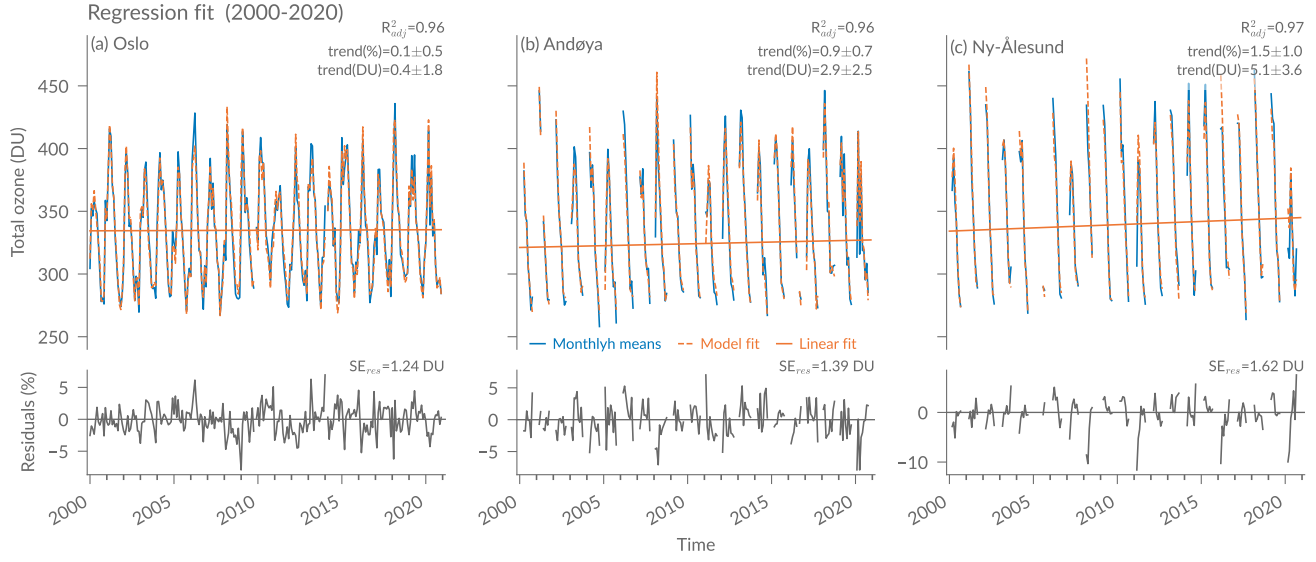

Figure 8. Regression fit of total ozone for **(a)** Oslo, **(b)** Andøya, and **(c)** Ny-Ålesund. The resulting linear trend is given in % per decade and DU per decade with 2-standard-deviation (σ) uncertainties. The lower panels show the residuals of the regression fit in percent ((Data–Model)/Data) and the standard error of the residuals (SE_{res}).

maxima. The rather stable February years in the beginning of the time series (2000-2003) coincide with the first maximum of the solar cycle, and higher ozone occurs again during the second solar maximum in the years 2013 and 2015. This may explain the strong contribution of the solar predictor to ozone in February at Oslo as visible in Fig. 7. Longer time series would need to be investigated to analyse this effect further. Interestingly, the Oslo February fit is remarkably good compared to other months, with a R^2_{adj} of 0.96 (see Fig. 7), indicating that the predictors used can well capture the high year-to-year variability in February.

Ozone trends in spring months are of special interest in polar regions, as they experienced strongest ozone depletion in the pre-2000 phase. At the two northernmost stations (Ny-Ålesund and Andøya), our analyses report positive but insignificant ozone trends in March and April. The trend uncertainties are high, related to the large interannual variability. In April, the model fit is less good than in most other months, with R^2_{adj} of 0.33 (Ny-Ålesund) and 0.49 (Andøya), indicating that April ozone variability is less well explained by the predictors used in our regression. In March, however, R^2_{adj} values are at least 0.86 at all three stations. The March time series and the corresponding regression fits are shown in Fig. 10. Even though the March trends are not significantly different from zero (at 95% confidence) due to large trend uncertainties, it is remarkable that all three station data agree on similar positive ozone trends of around 3% per decade and that the regression model can reproduce the ozone variability so well.

Our significant autumn trends confirm results by Svendby et al. (2021), who found significant trends at Oslo of 3.23±2.01% in fall from 1999 to 2019 using a simple linear regression. Positive but insignificant March trends in the Arctic (60° N to 90° N) have also been reported by Weber et al. (2018) based on zonal satellite and ground-based data, who found trends of 1.2±3.7%

https://doi.org/10.5194/acp-2022-488
Preprint. Discussion started: 18 July 2022

Atmospheric Chemistry and Physics Discussions

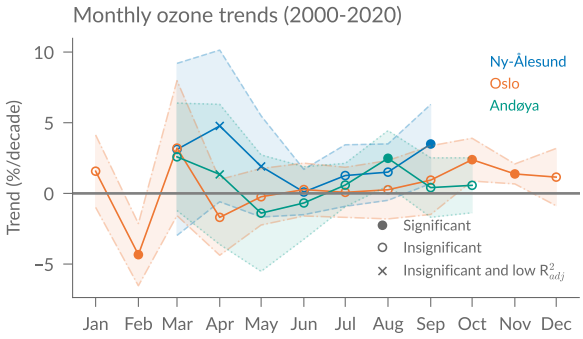

Figure 9. Monthly ozone trends in percent per decade for the three stations, with 2-σ uncertainty shadings. Filled dots represent trends that are significantly different from zero at the 95% confidence interval. Fits with low R^2_{adj} <0.5 are marked with crosses.

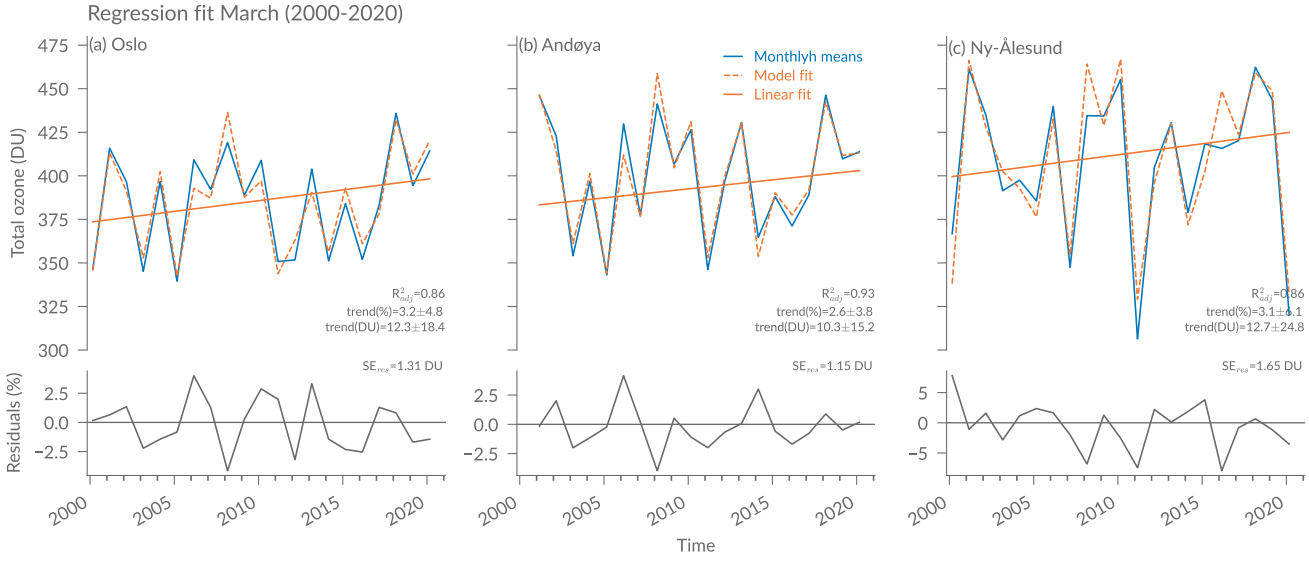

Figure 10. Same as Fig. 8 but for the month of March.

per decade (with 2-σ uncertainties) from 2000 to 2016 and slightly larger trends when extending to 2020 (2.0±3.9%, Weber et al. (2022)). Our March trends at the three stations are slightly larger than those zonal mean trends. These results confirm previous studies reporting zonally asymmetric trends with larger trends over the Atlantic and Scandinavian sector compared to other longitudes at northern high-latitudes (Zhang et al., 2019; Sofieva et al., 2021; Coldewey-Egbers et al., 2022).

https://doi.org/10.5194/acp-2022-488
Preprint. Discussion started: 18 July 2022


Atmospheric Chemistry and Physics Discussions

6 Conclusions

This study investigates ground-based total ozone trends at the northern high-latitude stations Oslo, Andøya and Ny-Ålesund. We presented combined total ozone time series at the three stations with measurements from four measurement techniques (Brewer DS, Brewer GI, SAOZ, and GUV). The combination of various techniques makes it possible to overcome measurement gaps due to instrumental limitations. The combined time series were compared with satellite overpass data and ERA5 reanalysis. All datasets agree on average within 1 to 3 % with the ground-based time series.

To derive total ozone trends from 2000 to 2020, we used the LOTUS regression model for the first time for ground-based total ozone data at high latitudes. Additional regression predictors have been examined and a set of predictors has been identified that should be considered when deriving total ozone trends at northern high-latitudes. We examined various predictors that are commonly used to account for natural ozone variability by checking their correlations and contributions to the regression fit. We found that tropopause pressure and lower-stratospheric temperature are dominant predictors that contribute significantly to ozone in most months. Our results further show that the trend model with the selected predictors represents well the total ozone variability at the selected stations, with generally high R^2_{adj}. We found significant trends of 0.9 % per decade at Andøya and 1.5% per decade at Ny-Ålesund, but no significant trends at Oslo when looking at the full time series. Our monthly regression analyses indicate significant positive trends in autumn at Oslo (October and November) and late summer at the northernmost stations Andøya and Ny-Ålesund (August or September). Finally, we observe positive trends of around 3% per decade in Arctic spring (March) but the trends are not significantly different from zero. Nevertheless, these springtime trends and the significant autumn trends might be an indication for Arctic ozone recovery due to changes in ODSs.

In conslusion, our study emphasizes the urgency to concentrate on regional ozone trends rather than zonal means when investigating Arctic ozone recovery. Long-term ground-based measurements of total ozone can contribute to this aim by verifying satellite-derived trends on a regional scale. Our results contribute to a better understanding of regional total ozone trends at northern high-latitudes, which is essential to assess how Arctic ozone responds to changes in ODSs and to climate change.

Data availability. The combined time series used in this study – including daily SAOZ means and noon measurements of Brewer DS, Brewer GI, and GUV – are provided at https://doi.org/10.5281/zenodo.6760259 (Bernet et al., 2022). The full Brewer GI data can be found at https://doi.org/10.5281/zenodo.6760244 (Svendby et al., 2022). The full time series of Brewer DS daily means are available at the World Ozone and Ultraviolet Radiation Data Centre (https://woudc.org). SAOZ data are available at http://www.ndaccdemo.org/. GUV data (v2.0) are available at https://doi.org/10.5281/zenodo.4773478 (Svendby, 2021), and are used here with some updates (extended to 2020, and calibrated in 2019 and 2020). OMI and GOME-2 overpass data are available at the Aura validation centre, for OMI (OMDOAO3) through https://avdc.gsfc.nasa.gov/pub/data/satellite/Aura/OMI/V03/L2OVP/OMDOAO3 (Veefkind, 2006, accessed 30.11.2021) and for GOME-2A and GOME-2B through https://avdc.gsfc.nasa.gov/pub/data/satellite/MetOp/GOME2/V03/L2OVP/. The SBUV MOD data are available at https://acd-ext.gsfc.nasa.gov/Data_services/merged/. The NCEP Reanalysis Derived data used for tropopause predictors were provided by the NOAA/OAR/ESRL PSL, Boulder, Colorado, USA, from their website at https://psl.noaa.gov/data/gridded/data.ncep.reanalysis.derived.tropopause.html. The other sources for the predictors used in the trend model are given in Table 1.

https://doi.org/10.5194/acp-2022-488
Preprint. Discussion started: 18 July 2022

Atmospheric Chemistry and Physics Discussions

Appendix A: Global irradiance (GI) method

A1 GI retrieval

The most accurate estimates of total ozone amount in the atmosphere with the Brewer spectrophotometer use direct sun (DS) measurements. The DS procedure is based on simultaneous measurements of direct solar radiation I_i at four UV wavelengths (i = 2,3,4,5) with different ozone absorption coefficients. The wavelenghts used are 310.1 nm, 313.5 nm, 316.8 nm, and 320.1 nm all with a 0.6 nm bandwidth (full width at half maximum, FWHM) (SCI-TEC Instruments, 1999). Combining the radiation at the four wavelengths we obtain:

$$N(x,\theta_s) = \frac{I_4(x,\theta_s)}{I_2(x,\theta_s)} \cdot \left(\frac{I_4(x,\theta_s)}{I_3(x,\theta_s)}\right)^{-0.5} \cdot \left(\frac{I_5(x,\theta_s)}{I_4(x,\theta_s)}\right)^{-1.7} \tag{A1}$$

where x is the ozone amount and θ_s is the solar zenith angle (SZA). The values -0.5 and -1.7 are weights that minimize effects of SO_2 absorption on $N(x,\theta_s)$. Radiances of direct sunlight passing through the atmosphere are attenuated according to Beer's law. As the ozone absorption coefficients and molecular scattering cross-sections for the different wavelengths used are known, the total ozone amount x can be found by taking the logarithm of N and considering the known absorption coefficients, the air mass factor and the background intensity (see e.g. Savastiouk and McElroy (2005), WMO (2008, Chapter 16), Fioletov et al. (2011)).

When clouds obscure the sun, the radiances I do not obey Beer's law because diffuse (scattered) radiation becomes important. Therefore, the simple logarithm procedure fails. In the GI (global irradiance) method, the radiances I in Eq. A1 are replaced by irradiances E, i.e. the sum of the direct and diffuse radiation falling on a flat horizontal surface. The global irradiances are measured through the UV dome of the Brewer instead of the flat quarts window used for DS measurements. The modified radiation for GI, $N_{GI}(x,\theta_s)$, is:

$$N_{GI}(x,\theta_s) = \frac{E_4(x,\theta_s)}{E_2(x,\theta_s)} \cdot \left(\frac{E_4(x,\theta_s)}{E_3(x,\theta_s)}\right)^{-0.5} \cdot \left(\frac{E_5(x,\theta_s)}{E_4(x,\theta_s)}\right)^{-1.7} \tag{A2}$$

The $N_{GI}(X,\theta_s)$ is simulated with a multiple scattering pseudo-spherical radiative transfer model (Stamnes et al., 1988; Dahlback and Stamnes, 1991) for various x and θ_s to obtain a lookup table. Light scattering on air molecules depends strongly on wavelength (Rayleigh scattering). In clouds, the wavelength dependency is considerably smaller due to the much larger sizes of cloud particles compared to air molecules (Mie scattering). Since the N_{GI}-values are based on irradiance ratios, the sensitivity to clouds is expected to be small, at least for thin clouds. Thus the lookup table is calculated for clear sky and a surface albedo of 5% pertinent for snow- and ice-free surfaces. The sensitivity of ozone profiles to the irradiances (and hence the N_{GI}-values) increases with θ_s. Therefore, a profile climatology for low, middle, or high latitudes (McPeters et al., 1998) can be chosen to compute the N_{GI}-value lookup tables. The ozone amount x is then determined by finding the N_{GI}-value in the lookup table that agrees with the observed N_{GI}.

https://doi.org/10.5194/acp-2022-488
Preprint. Discussion started: 18 July 2022


Atmospheric Chemistry and Physics Discussions

A2 GI calibration

The radiation detector in the Brewer is a photomultiplier tube (PMT). The irradiance for a particular wavelength is proportional to its count rate C_i (i = 2,3,4,5). The N_{GI}-value can be written as

$$N_{GI}(x,\theta_s) = r \cdot \frac{C_4(x,\theta_s)}{C_2(x,\theta_s)} \cdot \left(\frac{C_4(x,\theta_s)}{C_3(x,\theta_s)}\right)^{-0.5} \cdot \left(\frac{C_5(x,\theta_s)}{C_4(x,\theta_s)}\right)^{-1.7} \quad \text{(A3)}$$

where r is a calibration factor that is determined by utilizing a reliable ozone DS measurement with the Brewer. By choosing a day with clear sky, preferably around noon, the r value is determined such that Eq. A3 agrees with the N_{GI}-value in the lookup table for the observed DS ozone value and SZA θ_s. We performed a GI calibration as soon as we observed severe changes in the Brewer standard lamp (SL). In Andøya, we calibrated GI in 06-2001, 08-2014, 08-2016, 08-2018, and 08-2019 (see Fig. 2), for Oslo we used new calibration files in 08-2005 and twice in summer 2019.

The Oslo Brewer is equipped with a single monochromator. It is well known that stray light in the single Brewer optics causes errors in measured ozone at large θ_s and particularly for large ozone amounts. Therefore, for low sun (θ_s >72°) we replace the four-wavelength ratios in Eqs. A2 and A3 by a single ratio of 316.8 nm to 313.5 nm. The motivation for this is that we avoid 310.1 nm-radiation that is the wavelength that is mostly affected by stray light in Eq. A2.

In order to filter out cases where thick clouds are difficult to correct, we define a cloud transmission factor CLT:

$$CLT = cr \cdot \frac{C_{5,meas}(x,\theta_s)}{E_{5,clearsky}(x,\theta_s)} \quad \text{(A4)}$$

$C_{5,meas}$ is the measured irradiance (count rate), $E_{5,clearsky}$ is the clear-sky irradiance calculated with the radiative transfer model for a snow- and ice-free surface. The factor cr is a calibration factor that is determined by using measurements on a day with cloud-free and snow-free conditions with CLT = 1 (100%).

A3 GI processing

The GI method described above will normally work well without further corrections. However, to optimize the measurements, we have taken instrumental drift (SL changes) into account, as described in Sect. 2.1.1. for DS measurements. Further, we performed minor cloud- and SZA corrections, based on the comparison to DS measurements. Similar corrections have been used by Svendby et al. (2021) on measurements from ground-based UV (GUV) radiometers. The SZA correction is mainly relevant for the winter season when the combination of a changed atmospheric profile and low sun can introduce errors to the ozone value retrieved from the lookup table. To obtain corrected GI values (GI_{corr}), we derive a correction function $f(i)$ from the linear relationship between the DS/GI-ratio and the solar angle (i =SZA) as well as DS/GI and the cloud transmittance (i =CLT):

$$\mathrm{GI}_{corr}(t) = \mathrm{GI}(t) \cdot f(i) \quad \text{(A5)}$$

with

$$f(i) = \frac{\mathrm{DS}(i)}{\mathrm{GI}(i)} = a_i \cdot i + b_i. \quad \text{(A6)}$$

https://doi.org/10.5194/acp-2022-488
Preprint. Discussion started: 18 July 2022

Atmospheric Chemistry and Physics Discussions

Table A1. Linear fit between DS/GI-ratio and solar zenith angle (SZA) and cloud transmittance (CLT) used for the GI correction in Eq. A6.

Station	a_{SZA}	b_{SZA}	a_{CLT}	b_{CLT}
Oslo	3.9084×10^{-4}	0.9765	6.5914×10^{-4}	0.9501
Andøya	2.1208×10^{-4}	0.9848	2.7129×10^{-4}	0.9781

The GI is first corrected for the SZA dependence and the corrected data is then used to derive coefficients for the CLT-correction. The correction coefficients are derived by comparing GI to DS measurements from 1995 to 2020 in Oslo and from 2000 to 2020 in Andøya. The derived coefficients are given in Table A1. The CLT correction is only applied for cloudy situations (CLT$< 90\%$). Finally, we excluded GI data for situations with low cloud transmittance (CLT$< 20\%$) and situations with $\theta_s > 84°$.

https://doi.org/10.5194/acp-2022-488
Preprint. Discussion started: 18 July 2022

Atmospheric Chemistry and Physics Discussions

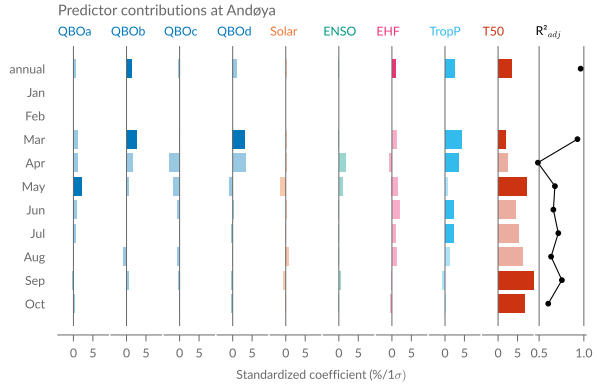

Figure B1. Predictor contribution to the regression fit at Andøya for the annual regression fit and individual monthly fits. The last panel on the right shows the adjusted coefficient of determination (R^2_{adj}) for the annual and all monthly fits.

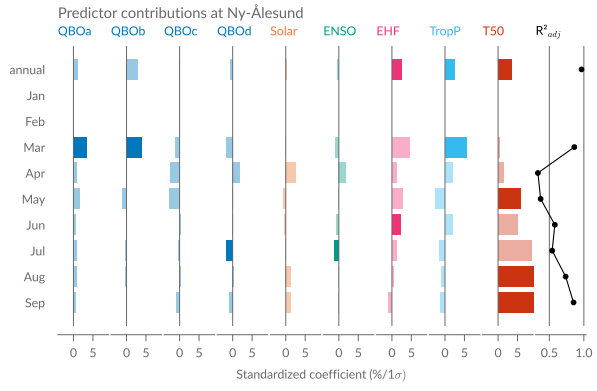

Figure B2. Same as Fig. B1 but for Ny-Ålesund.

Appendix B: Regression predictors at additional stations

Similar as Fig. 6 for Oslo, the following figures show the monthly contributions of predictors used in the regression model for Andøya (Fig. B1) and Ny-Ålesund (Fig. B2).

https://doi.org/10.5194/acp-2022-488
Preprint. Discussion started: 18 July 2022

Atmospheric Chemistry and Physics Discussions

Author contributions. The study concept was designed by LB and developed in collaboration with TS, the section on trend analyses were designed by LB, TS, GH and YO. The GI method (Appendix A) was described by AD with contributions by AK. AP and FG were responsible for the SAOZ data, and BP for the Brewer data at Ny-Ålesund. The data analysis and manuscript preparation was performed by LB. All authors contributed to the manuscript preparation and the interpretation of the results.

Competing interests. The authors declare that they have no conflict of interest.

Acknowledgements. This work was funded by the SNSF (Swiss National Science Foundation), grant no. 195484. We thank the Norwegian Environment Agency for funding the total ozone measurements. Many thanks to the LOTUS group for providing the regression model and to Daniel Zawada and Robert Damadeo for their helpful comments regarding the LOTUS regression.

https://doi.org/10.5194/acp-2022-488
Preprint. Discussion started: 18 July 2022

References

Anstey, J. A., Banyard, T. P., Butchart, N., Coy, L., Newman, P. A., Osprey, S., and Wright, C.: Prospect of increased disruption to the QBO in a changing climate, Earth and Space Science Open Archive, pp. 1–24, https://doi.org/10.1002/essoar.10503358.3, 2021.

Appenzeller, C., Weiss, A. K., and Staehelin, J.: North Atlantic Oscillation modulates total ozone winter trends, Geophysical Research Letters, 27, 1131–1134, https://doi.org/10.1029/1999GL010854, 2000.

Bahramvash Shams, S., Walden, V. P., Petropavlovskikh, I., Tarasick, D., Kivi, R., Oltmans, S., Johnson, B., Cullis, P., Sterling, C. W., Thölix, L., Errera, Q., Bahramvash Shams, S., Walden, V. P., Petropavlovskikh, I., Tarasick, D., Kivi, R., Oltmans, S., Johnson, B., Cullis, P., Sterling, C. W., Thölix, L., and Errera, Q.: Variations in the vertical profile of ozone at four high-latitude Arctic sites from 2005 to 2017, Atmospheric Chemistry and Physics, 19, 9733–9751, https://doi.org/10.5194/acp-19-9733-2019, iSBN: 1997332019, 2019.

Baldwin, M. P., Gray, L. J., Dunkerton, T. J., Hamilton, K., Haynes, P. H., Randel, W. J., Holton, J. R., Alexander, M. J., Hirota, I., Horinouchi, T., Jones, D. B. A., Kinnersley, J. S., Marquardt, C., Sato, K., and Takahashi, M.: The Quasi-Biennial Oscillation, Reviews of Geophysics, 39, 179–229, https://doi.org/http://dx.doi.org/10.1029/1999RG000073; doi:10.1029/1999RG000073, 2001.

Ball, W. T., Alsing, J., Staehelin, J., Davis, S. M., Froidevaux, L., and Peter, T.: Stratospheric ozone trends for 1985-2018: Sensitivity to recent large variability, Atmospheric Chemistry and Physics, 19, 12 731–12 748, https://doi.org/10.5194/acp-19-12731-2019, 2019.

Bernet, L., Boyd, I., Nedoluha, G., Querel, R., Swart, D., and Hocke, K.: Validation and trend analysis of stratospheric ozone data from ground-based observations at Lauder, New Zealand, Remote Sensing, 13, 1–15, https://doi.org/10.3390/rs13010109, 2021.

Bernet, L., Svendby, T., Hansen, G., Goutail, F., Pazmiño, A., and Petkov, B.: Combined ground-based total ozone data at three Norwegian sites (2000 to 2020) (version v1.0), https://doi.org/10.5281/zenodo.6760259, type: dataset, 2022.

Bernhard, G.: Real-time ultraviolet and column ozone from multichannel ultraviolet radiometers deployed in the National Science Foundation's ultraviolet monitoring network, Optical Engineering, 44, 041 011, https://doi.org/10.1117/1.1887195, 2005.

Bodeker, G. E. and Kremser, S.: Indicators of Antarctic ozone depletion: 1979 to 2019, Atmospheric Chemistry and Physics, 21, 5289–5300, https://doi.org/10.5194/acp-21-5289-2021, 2021.

Brönnimann, S., Luterbacher, J., Schmutz, C., Wanner, H., and Staehelin, J.: Variability of total ozone at Arosa, Switzerland, since 1931 related to atmospheric circulation indices, Geophysical Research Letters, 27, 2213–2216, https://doi.org/10.1029/1999GL011057, 2000.

Brunner, D., Staehelin, J., Maeder, J. A., Wohltmann, I., and Bodeker, G. E.: Variability and trends in total and vertically resolved stratospheric ozone based on the CATO ozone data set, Atmospheric Chemistry and Physics, 6, 4985–5008, https://doi.org/10.5194/acp-6-4985-2006, 2006.

Cochrane, D. and Orcutt, G. H.: Application of Least Squares Regression to Relationships Containing Auto-Correlated Error Terms, Journal of the American Statistical Association, 44, 32–61, https://doi.org/10.1080/01621459.1949.10483290, publisher: Taylor & Francis, 1949.

Coldewey-Egbers, M., Loyola, D. G., Lerot, C., and Van Roozendael, M.: Global, regional and seasonal analysis of total ozone trends derived from the 1995–2020 GTO-ECV climate data record, Atmospheric Chemistry and Physics, 22, 6861–6878, https://doi.org/10.5194/acp-22-6861-2022, publisher: Copernicus GmbH, 2022.

Dahlback, A. and Stamnes, K.: A new spherical model for computing the radiation field available for photolysis and heating at twilight, Planetary and Space Science, 39, 671–683, https://doi.org/10.1016/0032-0633(91)90061-E, 1991.

Damadeo, R. P., Zawodny, J. M., and Thomason, L. W.: Reevaluation of stratospheric ozone trends from SAGE II data using a simultaneous temporal and spatial analysis, Atmospheric Chemistry and Physics, 14, 13 455–13 470, https://doi.org/10.5194/acp-14-13455-2014, 2014.

https://doi.org/10.5194/acp-2022-488
Preprint. Discussion started: 18 July 2022

De Laat, A. T., Van Der A, R. J., and Van Weele, M.: Tracing the second stage of ozone recovery in the Antarctic ozone-hole with a "big data" approach to multivariate regressions, Atmospheric Chemistry and Physics, 15, 79–97, https://doi.org/10.5194/acp-15-79-2015, 2015.

Fioletov, V. E. and Shepherd, T. G.: Seasonal persistence of midlatitude total ozone anomalies, Geophys. Res. Lett., 30, https://doi.org/10.1029/2002GL016739, 2003.

Fioletov, V. E., McLinden, C. A., McElroy, C. T., and Savastiouk, V.: New method for deriving total ozone from Brewer zenith sky observations, Journal of Geophysical Research Atmospheres, 116, 1–10, https://doi.org/10.1029/2010JD015399, 2011.

Frith, S. M., Kramarova, N. A., Stolarski, R. S., McPeters, R. D., Bhartia, P. K., and Labow, G. J.: Recent changes in total column ozone based on the SBUV Version 8.6 Merged Ozone Data Set, Journal of Geophysical Research: Atmospheres, 119, 9735–9751, https://doi.org/10.1002/2014JD021889, iSBN: 2169-8996, 2014.

Gabriel, A. and Schmitz, G.: The Influence of Large-Scale Eddy Flux Variability on the Zonal Mean Ozone Distribution, J. Climate, 16, 2615–2627, https://doi.org/10.1175/1520-0442(2003)016<2615:TIOLEF>2.0.CO;2, 2003.

Godin-Beekmann, S., Azouz, N., Sofieva, V., Hubert, D., Petropavlovskikh, I., Effertz, P., Ancellet, G., Degenstein, D. A., Zawada, D., Froidevaux, L., Wild, J., Davis, S., Steinbrecht, W., Leblanc, T., and Querel, R.: Updated trends of the stratospheric ozone vertical distribution in the 60 ° S-60 ° N latitude range based on the LOTUS regression model, Atmospheric Chemistry and Physics Discussions, pp. 1–28, 2022.

Goutail, F., Pommereau, J. P., Lefèvre, F., Van Roozendael, M., Andersen, S. B., Kåstad Høiskar, B. A., Dorokhov, V., Kyrö, E., Chipperfield, M. P., and Feng, W.: Early unusual ozone loss during the Arctic winter 2002/2003 compared to other winters, Atmospheric Chemistry and Physics, 5, 665–677, https://doi.org/10.5194/acp-5-665-2005, 2005.

Hansen, G. and Svenøe, T.: Multilinear regression analysis of the 65-year Tromsø total ozone series, Journal of Geophysical Research D: Atmospheres, 110, 1–11, https://doi.org/10.1029/2004JD005387, 2005.

Hendrick, F., Pommereau, J. P., Goutail, F., Evans, R. D., Ionov, D., Pazmino, A., Kyró, E., Held, G., Eriksen, P., Dorokhov, V., Gil, M., and Van Roozendael, M.: NDACC/SAOZ UV-visible total ozone measurements: Improved retrieval and comparison with correlative ground-based and satellite observations, Atmospheric Chemistry and Physics, 11, 5975–5995, https://doi.org/10.5194/acp-11-5975-2011, 2011.

Hersbach, H., Bell, B., Berrisford, P., Biavati, G., Horányi, A., Muñoz Sabater, J., Nicolas, J., Peubey, C., Radu, R., Rozum, I., Schepers, D., Simmons, A., Soci, C., Dee, D., and Thépaut, J.-N.: ERA5 hourly data on single levels from 1979 to present, Copernicus Climate Change Service (C3S) Climate Data Store (CDS), https://doi.org/10.24381/cds.adbb2d47, 2018.

Hersbach, H., Bell, B., Berrisford, P., Biavati, G., Horányi, A., Muñoz Sabater, J., Nicolas, J., Peubey, C., Radu, R., Rozum, I., Schepers, D., Simmons, A., Soci, C., Dee, D., and Thépaut, J.-N.: ERA5 monthly averaged data on pressure levels from 1979 to present, Copernicus Climate Change Service (C3S) Climate Data Store (CDS), https://doi.org/10.24381/cds.6860a573, 2019.

Hersbach, H., Bell, B., Berrisford, P., Hirahara, S., Horányi, A., Muñoz-Sabater, J., Nicolas, J., Peubey, C., Radu, R., Schepers, D., Simmons, A., Soci, C., Abdalla, S., Abellan, X., Balsamo, G., Bechtold, P., Biavati, G., Bidlot, J., Bonavita, M., Chiara, G., Dahlgren, P., Dee, D., Diamantakis, M., Dragani, R., Flemming, J., Forbes, R., Fuentes, M., Geer, A., Haimberger, L., Healy, S., Hogan, R. J., Hólm, E., Janisková, M., Keeley, S., Laloyaux, P., Lopez, P., Lupu, C., Radnoti, G., Rosnay, P., Rozum, I., Vamborg, F., Villaume, S., and Thépaut, J.-N.: The ERA5 global reanalysis, Quarterly Journal of the Royal Meteorological Society, 146, 1999–2049, https://doi.org/10.1002/qj.3803, 2020.

Kalnay, E., Kanamitsu, M., Kistler, R., Collins, W., Deaven, D., Gandin, L., Iredell, M., Saha, S., White, G., Woollen, J., Zhu, Y., Leetmaa, A., Reynolds, R., Chelliah, M., Ebisuzaki, W., Higgins, W., Janowiak, J., Mo, K. C., Ropelewski, C., Wang, J., Jenne, R., and Joseph, D.: The

https://doi.org/10.5194/acp-2022-488
Preprint. Discussion started: 18 July 2022

NCEP/NCAR 40-Year Reanalysis Project, Bulletin of the American Meteorological Society, 77, 437–471, https://doi.org/10.1175/1520-0477(1996)077<0437:TNYRP>2.0.CO;2, 1996.

Knibbe, J. S., Van Der A, R. J., and De Laat, A. T.: Spatial regression analysis on 32 years of total column ozone data, Atmospheric Chemistry and Physics, 14, 8461–8482, https://doi.org/10.5194/acp-14-8461-2014, 2014.

Kuttippurath, J. and Nair, P. J.: The signs of Antarctic ozone hole recovery, Scientific Reports, 7, https://doi.org/10.1038/s41598-017-00722-7, 2017.

Kuttippurath, J., Godin-Beekmann, S., Lefèvre, F., Santee, M. L., Froidevaux, L., and Hauchecorne, A.: Variability in Antarctic ozone loss in the last decade (2004-2013): High-resolution simulations compared to Aura MLS observations, Atmospheric Chemistry and Physics, 15, 10 385–10 397, https://doi.org/10.5194/acp-15-10385-2015, 2015.

Langematz, U., Tully, M., Calvo, N., Dameris, M., Laat, J., Klekociuk, A., Müller, R., and Young, P.: Polar stratospheric ozone: Past, present, and future, Chapter 4 in WMO scientific Assessment of Ozone Depletion: 2018, in: Scientific Assessment of Ozone Depletion: 2018, Global Ozone Research and Monitoring Project – Report No. 58, vol. 58, World Meteorological Organization, Geneva, Switzerland, 2018.

Lee, H.: Simulation of the combined effects of solar cycle, quasi-biennial oscillation, and volcanic forcing on stratospheric ozone changes in recent decades, J. Geophys. Res., 108, 4049, https://doi.org/10.1029/2001JD001503, 2003.

Mäder, J. A., Staehelin, J., Brunner, D., Stahel, W. A., Wohltmann, I., and Peter, T.: Statistical modeling of total ozone: Selection of appropriate explanatory variables, Journal of Geophysical Research Atmospheres, 112, 1–16, https://doi.org/10.1029/2006JD007694, 2007.

McPeters, R. D., Bhartia, P. K., Krueger, A. J., Herman, J. R., Wellemeyer, C. G., Seftor, C. J., Jaross, G., Torres, O., Moy, L., Labow, G., Byerly, W., Taylor, S. L., Swissler, T., and Cebula, R. P.: Earth Probe Total Ozone Mapping Spectrometer (TOMS) Data Products User's Guide, Tech. Rep. 1998-206895, National Aeronautics and Space Administration, Goddard Space Flight Center, Lanham, Maryland, USA, 1998.

Meng, L., Liu, J., Tarasick, D. W., Randel, W. J., Steiner, A. K., Wilhelmsen, H., Wang, L., and Haimberger, L.: Continuous rise of the tropopause in the Northern Hemisphere over 1980–2020, Science Advances, 7, eabi8065, https://doi.org/10.1126/sciadv.abi8065, publisher: American Association for the Advancement of Science, 2021.

Newman, P. A., Daniel, J. S., Waugh, D. W., and Nash, E. R.: A new formulation of equivalent effective stratospheric chlorine (EESC), Atmospheric Chemistry and Physics, 7, 4537–4552, https://doi.org/10.5194/acp-7-4537-2007, 2007.

Oman, L. D., Douglass, A. R., Ziemke, J. R., Rodriguez, J. M., Waugh, D. W., and Nielsen, J. E.: The ozone response to ENSO in Aura satellite measurements and a chemistry-climate simulation: OZONE RESPONSE TO ENSO, J. Geophys. Res. Atmos., 118, 965–976, https://doi.org/10.1029/2012JD018546, 2013.

Orsolini, Y. J. and Doblas-Reyes, F. J.: Ozone signatures of climate patterns over the Euro-Atlantic sector in the spring, Quarterly Journal of the Royal Meteorological Society, 129, 3251–3263, https://doi.org/10.1256/qj.02.165, 2003.

Pazmiño, A., Godin-Beekmann, S., Hauchecorne, A., Claud, C., Khaykin, S., Goutail, F., Wolfram, E., Salvador, J., and Quel, E.: Multiple symptoms of total ozone recovery inside the Antarctic vortex during austral spring, Atmospheric Chemistry and Physics, 18, 7557–7572, https://doi.org/10.5194/acp-18-7557-2018, 2018.

Plumb, R. A.: Stratospheric transport, Journal of the Meteorological Society of Japan, 80, 793–809, https://doi.org/10.2151/jmsj.80.793, 2002.

Pommereau, J. P. and Goutail, F.: O3 and NO2 ground-based measurements by visible spectrometry during Arctic winter and spring 1988, Geophysical Research Letters, 15, 891–894, https://doi.org/https://doi.org/10.1029/GL015i008p00891, 1988.

https://doi.org/10.5194/acp-2022-488
Preprint. Discussion started: 18 July 2022

Atmospheric Chemistry and Physics Discussions

Savastiouk, V. and McElroy, C. T.: Brewer spectrophotometer total ozone measurements made during the 1998 Middle Atmosphere Nitrogen Trend Assessment (MANTRA) Campaign, Atmosphere - Ocean, 43, 315–324, https://doi.org/10.3137/ao.430403, 2005.

Schuenemeyer, J. H. and Drew, L. J.: Regression, in: Statistics for Earth and Environmental Scientists, pp. 99–149, John Wiley & Sons, Ltd, Hoboken, New Jersey, https://doi.org/10.1002/9780470650707.ch4, 2010.

SCI-TEC Instruments: BREWER MKIV Spectrophotometer Operator's Manual, Tech. Rep. OM-BA-C231 REV B, SCI-TEC Instruments Inc., Saskatoon, Sask., Canada, 1999.

Sofieva, V. F., Szelag, M., Tamminen, J., Kyro¨la¨, E., Degenstein, D., Roth, C., Zawada, D., Rozanov, A., Arosio, C., Burrows, J. P., Weber, M., Laeng, A., Stiller, G. P., Von Clarmann, T., Froidevaux, L., Livesey, N., Van Roozendael, M., and Retscher, C.: Measurement report: Regional trends of stratospheric ozone evaluated using the MErged GRIdded Dataset of Ozone Profiles (MEGRIDOP), Atmospheric Chemistry and Physics, 21, 6707–6720, https://doi.org/10.5194/acp-21-6707-2021, 2021.

Solomon, S., Portmann, R. W., Garcia, R. R., Randel, W., Wu, F., Nagatani, R., Gleason, J., Thomason, L., Poole, L. R., and McCormick, M. P.: Ozone depletion at mid-latitudes: Coupling of volcanic aerosols and temperature variability to anthropogenic chlorine, Geophys. Res. Lett., 25, 1871–1874, https://doi.org/10.1029/98GL01293, 1998.

Solomon, S., Ivy, D. J., Kinnison, D., Mills, M. J., Neely, R. R., and Schmidt, A.: Emergence of healing in the Antarctic ozone layer, Science, 353, 269–274, https://doi.org/10.1126/science.aae0061, 2016.

SPARC/IO3C/GAW: SPARC/IO3C/GAW Report on Long-term Ozone Trends and Uncertainties in the Stratosphere, SPARC Report No. 9, GAW Report No. 241, WCRP-17/2018, https://doi.org/10.17874/f899e57a20b, 2019.

Stamnes, K., Tsay, S.-C., Wiscombe, W., and Jayaweera, K.: Numerically stable algorithm for discrete-ordinate-method radiative transfer in multiple scattering and emitting layered media, Appl. Opt., 27, 2502, https://doi.org/10.1364/AO.27.002502, 1988.

Steinbrecht, W., Claude, H., Köhler, U., and Hoinka, K. P.: Correlations between tropopause height and total ozone: Implications for long-term changes, Journal of Geophysical Research Atmospheres, 103, 19 183–19 192, https://doi.org/10.1029/98JD01929, 1998.

Svendby, T.: GUV total ozone column and effective cloud transmittance from three Norwegian sites 1995-2019 (Version v2.0), https://doi.org/10.5281/zenodo.4773478, type: dataset, 2021.

Svendby, T., Bernet, L., and Dahlback, A.: Brewer Global Iradiance (GI) total ozone data at two Norwegian sites (2000 to 2020) (version v1.0), https://doi.org/10.5281/zenodo.6760244, type: dataset, 2022.

Svendby, T. M. and Dahlback, A.: Statistical analysis of total ozone measurements in Oslo, Norway, 1978–1998, Journal of Geophysical Research, 109, 1–11, https://doi.org/10.1029/2004jd004679, 2004.

Svendby, T. M., Johnsen, B., Kylling, A., Dahlback, A., Bernhard, G., Hansen, G., Petkov, B., and Vitale, V.: GUV long-term measurements of total ozone column and effective cloud transmittance at three Norwegian sites, Atmospheric Chemistry and Physics Discussions, pp. 1–29, https://doi.org/10.5194/acp-21-7881-2021, 2021.

Thompson, A. M., Stauffer, R. M., Wargan, K., Witte, J. C., Kollonige, D. E., and Ziemke, J. R.: Regional and Seasonal Trends in Tropical Ozone From SHADOZ Profiles: Reference for Models and Satellite Products, JGR Atmospheres, 126, https://doi.org/10.1029/2021JD034691, 2021.

Tiao, G. C., Reinsel, G. C., Xu, D., Pedrick, J. H., Zhu, X., Miller, A. J., DeLuisi, J. J., Mateer, C. L., and Wuebbles, D. J.: Effects of autocorrelation and temporal sampling schemes, Journal of Geophysical Research, 95, 20 507–20 517, 1990.

Tung, K. K. and Yang, H.: Global QBO in Circulation and Ozone. Part I: Reexamination of Observational Evidence, Journal of the Atmospheric Sciences, 51, 2699–2707, https://doi.org/10.1175/1520-0469(1994)051<2699:GQICAO>2.0.CO;2, 1994.

USask ARG and LOTUS Group: LOTUS regression, https://arg.usask.ca/docs/LOTUS_regression/, 2017.

https://doi.org/10.5194/acp-2022-488
Preprint. Discussion started: 18 July 2022

Van Malderen, R., De Muer, D., De Backer, H., Poyraz, D., Verstraeten, W. W., De Bock, V., Delcloo, A. W., Mangold, A., Laffineur, Q., Allaart, M., Fierens, F., and Thouret, V.: Fifty years of balloon-borne ozone profile measurements at Uccle, Belgium: A short history, the scientific relevance, and the achievements in understanding the vertical ozone distribution, Atmospheric Chemistry and Physics, 21, 12 385–12 411, https://doi.org/10.5194/acp-21-12385-2021, 2021.

Varotsos, C., Cartalis, C., Vlamakis, A., Tzanis, C., and Keramitsoglou, I.: The long-term coupling between column ozone and tropopause properties, Journal of Climate, 17, 3843–3854, https://doi.org/10.1175/1520-0442(2004)017<3843:TLCBCO>2.0.CO;2, 2004.

Veefkind, P.: OMI/Aura Ozone (O3) DOAS Total Column 1-Orbit L2 Swath 13x24 km V003, Goddard Earth Sciences Data and Information Services Center (GES DISC), Greenbelt, MD, USA, https://doi.org/10.5067/Aura/OMI/DATA2012, 2006.

von der Gathen, P., Kivi, R., Wohltmann, I., Salawitch, R. J., and Rex, M.: Climate change favours large seasonal loss of Arctic ozone, Nature Communications, 12, https://doi.org/10.1038/s41467-021-24089-6, publisher: Springer US, 2021.

Wang, W., Hong, J., Shangguan, M., Wang, H., Jiang, W., and Zhao, S.: Zonally Asymmetric Influences of the Quasi-Biennial Oscillation on Stratospheric Ozone, Atmospheric Chemistry and Physics Discussions, pp. 1–26, https://doi.org/https://doi.org/10.5194/acp-2022-174, 2022.

Weber, M., Coldewey-Egbers, M., Fioletov, V. E., Frith, S. M., Wild, J. D., Burrows, J. P., Long, C. S., and Loyola, D.: Total ozone trends from 1979 to 2016 derived from five merged observational datasets – the emergence into ozone recovery, Atmospheric Chemistry and Physics, 18, 2097–2117, https://doi.org/10.5194/acp-18-2097-2018, 2018.

Weber, M., Arosio, C., Coldewey-Egbers, M., Fioletov, V. E., Frith, S. M., Wild, J. D., Tourpali, K., Burrows, J. P., and Loyola, D.: Global total ozone recovery trends attributed to ozone-depleting substance (ODS) changes derived from five merged ozone datasets, Atmos. Chem. Phys., 22, 6843–6859, https://doi.org/10.5194/acp-22-6843-2022, 2022.

WMO: Guide to meteorological instruments and methods of observation, WMO-NO. 8, World Meteorological Organization, Geneva, Switzerland, 7 edn., 2008.

WMO: Scientific Assessment of Ozone Depletion: 2018, p. 588, World Meteorological Organization, Global Ozone Research and Monitoring Project - Report No. 58, Geneva, Switzerland, 2018.

Wohltmann, I., Rex, M., Brunner, D., and Mäder, J.: Integrated equivalent latitude as a proxy for dynamical changes in ozone column, Geophysical Research Letters, 32, 1–4, https://doi.org/10.1029/2005GL022497, 2005.

Zhang, J., Tian, W., Xie, F., Sang, W., Guo, D., Chipperfield, M., Feng, W., and Hu, D.: Zonally asymmetric trends of winter total column ozone in the northern middle latitudes, Clim Dyn, 52, 4483–4500, https://doi.org/10.1007/s00382-018-4393-y, 2019.